Journal of ELECTRONIC MATERIALS, Vol. 48, No. 1, 2019
https://doi.org/10.1007/s11664-018-6786-4
© 2018 The Minerals, Metals & Materials Society

TMS2018 MICROELECTRONIC PACKAGING, INTERCONNECT, AND PB-FREE SOLDER

# Modeling and Experimental Verification of Intermetallic Compounds Grown by Electromigration and Thermomigration for Sn-0.7Cu Solders

SUNG-MIN BAEK,[1] YUJIN PARK,[2] CHEOLMIN OH,[3] EUN-JOON CHUN,[4] and NAMHYUN KANG[2,5]

1.—Samsung Electro-Mechanics, Seobuk-gu, Cheonan-si, Chungcheongnam-do 31086, Republic of Korea. 2.—Department of Materials Science and Engineering, Pusan National University, Busan 46241, Republic of Korea. 3.—Korea Electronics Technology Institute, Seongnam, Gyeonggi-do 13509, Republic of Korea. 4.—Busan Machinery Research Center, Korea Institute of Machinery and Materials, Busan 46744, Republic of Korea. 5.—e-mail: nhkang@pusan.ac.kr

Printed circuit boards that use fine pitch technology have a greater risk of open-circuit failure, due to void formations caused by the growth of intermetallic compounds. This failure mode is reported to be a result of electromigration (EM) damage. Current stressing occurs when current flows in a solder bump, thereby producing EM. Joule heating is also a significant occurrence under current stressing conditions, and induces thermomigration (TM) in solder bumps during EM. This study investigated the intermetallic compound (IMC) growth kinetics for Sn-0.7Cu solders, modeled by EM, TM, and chemical diffusion. The modeling results concurred with the observed kinetics of IMC growth. Electromigration influenced the growth of IMCs most significantly for a current density of 10 kA/cm$^2$. The effect of TM on the IMC growth had to be considered for a thermogradient of 870°C/cm. However, the effect of chemical diffusion was insignificant on IMC growth, specifically for a current density of 10 kA/cm$^2$.

**Key words:** Electromigration, thermomigration, Sn-0.7Cu solder, intermetallic compounds, modeling

## INTRODUCTION

The increase in the amount of data processed by microchips requires a growing number of I/O (input and output) pins for the chip to receive and send data. Furthermore, the miniaturization of printed circuit boards (PCBs) has resulted in a decrease in the size of solder bumps and an increase in the current density. The high current density at $\mu$-ball grid arrays ($\mu$-BGA) in package-on-package (PoP) devices raises serious concerns, which include open-circuit failure. This phenomenon occurs because electromigration (EM) accelerates the formation of Kirkendall voids and intermetallic compound (IMC) growth at the solder bump joint.[1] For EM, electrons from Al traces cause intensive joule heating in the solder bump of the chip, and this solder bump finally has a higher temperature than the substrate. Different temperatures across a solder bump produce a thermogradient, which induces thermomigration (TM) in the solder alloying elements, such as Cu and Sn atoms.[2,3]

IMC formation is related to the reliability of $\mu$-BGA, and the low mobility of Cu and Sn atoms in IMCs accelerates void formation at the solder joint.[4,5] The studies on IMC growth conducted by Chao and Chae et al. were focused on EM.[6,7] Their models predicted IMC growth by EM, and chemical diffusion in the solder bump. Moreover, various

(Received May 4, 2018; accepted November 1, 2018; published online November 26, 2018)

experimental studies observed IMC growth by EM,[8,9] and long-time annealing.[10–13]

Most studies on IMC growth induced by EM dealt with Sn-Ag and Sn-Ag-Cu solders such as Sn-3.5Ag, Sn-3Ag-0.5Cu, Sn-3.8Ag-0.7Cu, and Sn-3.5Ag-0.5Cu.[7,13,14] Specifically, studies on TM in Sn-0.7Cu solders are rare. Because practical solder bumps have a smaller area than a Cu pad,[6] both EM and TM affect IMC growth, and their respective roles are difficult to clarify.[15] Furthermore, there are no studies where the effects of EM, TM, and chemical diffusion have been effectively separated.

In this study, experiments were conducted to separate EM and TM, using the same cross-sectional areas of solder bump and Cu pad. They were compared by the modeling of IMC growth. Moreover, the effects of chemical diffusion, EM, and TM on IMC ($Cu_6Sn_5$, $Cu_3Sn$) growth, were compared in scale for Sn-0.7Cu solders.

## MODELING AND EXPERIMENTAL PROCEDURES

### Modeling of EM, TM, and Chemical Diffusion for $Cu_3Sn$ and $Cu_6Sn_5$ Growth

The IMCs formed in Sn-0.7Cu solder are $Cu_3Sn$ and $Cu_6Sn_5$. IMC growth was modeled for EM and TM. For EM, Cu and Sn atoms move due to EM momentum, when electrons transfer from the Cu pad to the solder. For TM, Cu and Sn atoms move due to heat flux momentum, caused by the thermogradient that occurs when the temperature of the Cu pad is higher than that of the solder.

For EM, atomic flux (J), caused by electron momentum, is written as follows[6,16]:

$$J_{\mathrm{Cu},i} = C_{\mathrm{Cu},i}\frac{D_{\mathrm{Cu},i}}{\mathrm{kT}}Z^{*}_{\mathrm{Cu},i}e\rho j$$
$$J_{\mathrm{Sn},i} = C_{\mathrm{Sn},i}\frac{D_{\mathrm{Sn},i}}{\mathrm{kT}}Z^{*}_{\mathrm{Sn},i}e\rho j \tag{1}$$

where $D$ is the diffusion coefficient, $k$ is the Boltzmann constant, $T$ is the absolute temperature, $Z^{*}$ is the effective charge number, $e$ is the electric charge quantity, $\rho$ is the resistivity, $i$ is each phase, and $j$ is the current density. $C$ is defined as the number of atoms per unit volume (atomic concentration) and is shown as follows:

$$C_i = C_0 n_i \tag{2}$$

where $C_0$ is the atomic density of each phase, and $n_i$ is the atomic fraction of each phase ($i$).

For TM, atomic flux caused by heat flux is expressed as follows[17]:

$$J_{\mathrm{Cu},i} = C_{\mathrm{Cu},i}\frac{D_{\mathrm{Cu},i}}{\mathrm{kT}}\frac{Q^{*}_{\mathrm{Cu}}}{T}\left(-\frac{\partial T}{\partial x}\right)$$
$$J_{\mathrm{Sn},i} = C_{\mathrm{Sn},i}\frac{D_{\mathrm{Sn},i}}{\mathrm{kT}}\frac{Q^{*}_{\mathrm{Sn}}}{T}\left(-\frac{\partial T}{\partial x}\right) \tag{3}$$

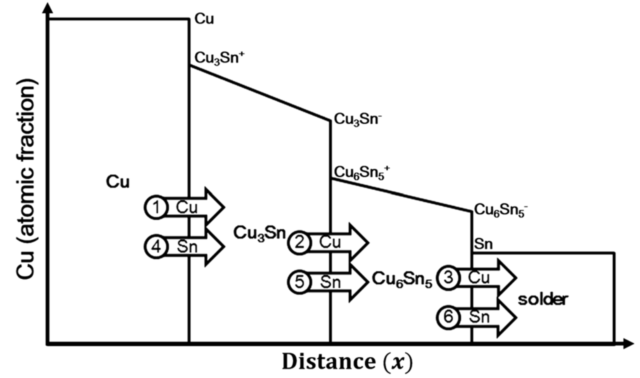


Fig. 1. Atomic fraction gradient between a Cu pad and the solder.

where $\left(-\frac{\mathrm{d}T}{\mathrm{d}x}\right)$ is the thermogradient and $Q^{*}$ is the heat of transport, which means the minimum enthalpy for atoms to transfer from the lattice site in isothermal transport. Figure 1 shows the atomic concentration of Cu atoms, following the equilibrium phase diagram of Cu-Sn binary alloys at 150°C. Table I shows the atomic fractions for the compositional boundary of each IMC. In Fig. 1 and Table 1, Cu means the Cu concentration of the Cu pad at the boundary between Cu and $Cu_3Sn$, and $Cu_3Sn^+$ is the Cu concentration of $Cu_3Sn$ at the boundary between Cu and $Cu_3Sn$. $Cu_3Sn^-$ is the Cu concentration of $Cu_3Sn$ at the boundary between $Cu_3Sn$ and $Cu_6Sn_5$, and $Cu_6Sn_5^+$ is the Cu concentration of $Cu_6Sn_5$ at the boundary between $Cu_3Sn$ and $Cu_6Sn_5$. $Cu_6Sn_5^-$ signifies the Cu concentration of $Cu_6Sn_5$ at the boundary between $Cu_6Sn_5$ and the solder, and Sn is the Cu concentration of Sn at the border between $Cu_6Sn_5$ and the solder.

In real situations, the concentration profile changes with time. The changes of the concentration profile can be described by Fick's second law:

$$\frac{\partial \mathrm{C}}{\partial \mathrm{t}} = -\frac{\partial J}{\partial x} \tag{4}$$

Since the compositional gap across the boundary of each phase (Cu versus $Cu_3Sn^+$, $Cu_3Sn^-$ versus $Cu_6Sn_5^+$, and $Cu_6Sn_5^-$ versus Sn) affects both the atomic flux ($J$) and concentration of Cu and Sn ($n_i$), the differences of concentration and flux are substituted into Eq. 4. Therefore, the atomic flux velocities affected respectively by EM and TM are calculated as follows:

$$v^{\mathrm{EM}}_{\mathrm{Cu}} = \frac{\mathrm{d}x}{\mathrm{d}t} = \frac{1}{C_{\mathrm{Cu,Cu}} - C_{\mathrm{Cu,Cu_3Sn^+}}}\frac{\mathrm{ej}}{\mathrm{kT}} \times \left[\begin{array}{l} C_{\mathrm{Cu,Cu}}\left(1 - n_{\mathrm{Cu,Cu}}\right)\left(D_{\mathrm{Sn,Cu}}Z^{*}_{\mathrm{Sn,Cu}} - D_{\mathrm{Cu,Cu}}Z^{*}_{\mathrm{Cu,Cu}}\right)\rho_{\mathrm{Cu}} \\ -C_{\mathrm{Cu,Cu_3Sn}}\left(1 - n_{\mathrm{Cu,Cu_3Sn}}\right)\left(D_{\mathrm{Sn,Cu_3Sn}}Z^{*}_{\mathrm{Sn,Cu_3Sn}} - D_{\mathrm{Cu,Cu_3Sn}}Z^{*}_{\mathrm{Cu,Cu_3Sn}}\right)\rho_{\mathrm{Cu_3Sn}} \end{array}\right] \tag{5}$$

$$v_{Cu}^{TM} = \frac{dx}{dt} = \frac{1}{C_{Cu,Cu} - C_{Cu,Cu_3Sn^+}} \left( -\frac{dT}{dx} \right) \frac{1}{kT^2} \times \begin{bmatrix} C_{Cu,Cu}(1 - n_{Cu,Cu})(D_{Sn,Cu}Q_{Sn}^* - D_{Cu,Cu}Q_{Cu}^*) \\ -C_{Cu,Cu_3Sn}(1 - n_{Cu,Cu_3Sn})(D_{Sn,Cu_3Sn}Q_{Sn}^* - D_{Cu,Cu_3Sn}Q_{Cu}^*) \end{bmatrix} \quad (6)$$

Equation 5 represents the flux velocity of a Cu atom that is transferred by EM from the Cu phase to the $Cu_3Sn$ phase. Equation 6 indicates the flux velocity of a Cu atom that transferred by TM from the Cu phase to the $Cu_3Sn$ phase. Equations 5 and 6 are the flux velocities of a Cu atom, noted with arrow ① in Fig. 1. In addition, the flux velocity of a Sn atom is calculated through the same procedure, using Eqs. 5 and 6. Finally, the growth velocity of $Cu_3Sn$ is calculated by adding ①, ②, ④, and ⑤ of Fig. 1, and that of $Cu_6Sn_5$ is calculated by adding ②, ③, ⑤, and ⑥ of Fig. 1.

Chemical diffusion occurs due to the concentration difference of Sn and Cu atoms, with respect to location. Figure 2 shows the concentration variation of Sn and Cu atoms from the Cu pad to the solder. The Cu atom moves from the pad, which has a high concentration of Cu, to the solder, which has a low concentration of Cu. However, the Sn atom moves from the solder to the Cu pad. Atomic flux ($J$), caused by the concentration gradient of Cu and Sn atoms, is written as follows:

**Table I. Cu atomic fraction determined from the phase diagram of Sn-Cu binary alloy[18]**

| Cu | $Cu_3Sn^+$ | $Cu_3Sn^-$ | $Cu_6Sn_5^+$ | $Cu_6Sn_5^-$ | Sn |
|---|---|---|---|---|---|
| 0.993 | 0.765 | 0.755 | 0.549 | 0.541 | 0.007 |

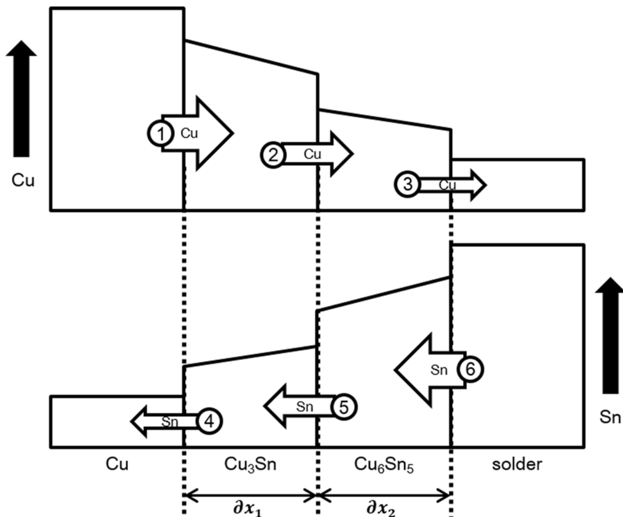


Fig. 2. Schematic diagram of Cu and Sn atom movements induced by chemical diffusion.

$$J_{Cu,i} = -D_{Cu,i}\frac{\partial C_{Cu,i}}{\partial x} \qquad J_{Sn,i} = -D_{Sn,i}\frac{\partial C_{Sn,i}}{\partial x} \quad (7)$$

Considering the concentration variation with respect to time, Eqs. 8 and 9 are obtained after applying Eqs. 7 to 4 as follows:

$$v_{Cu}^{CHE} = \frac{dx}{dt} = \frac{1}{C_{Cu,Cu} - C_{Cu,Cu_3Sn^+}} \times \begin{bmatrix} (n_{Sn,Cu}D_{Cu,Cu} + n_{Cu,Cu}D_{Sn,Cu})\frac{\partial C_{Cu,Cu}}{\partial x_{Cu}} \\ -(n_{Sn,Cu_3Sn}D_{Cu,Cu_3Sn} + n_{Cu,Cu_3Sn}D_{Sn,Cu_3Sn})\frac{\partial C_{Cu,Cu_3Sn}}{\partial x_{Cu_3Sn}} \end{bmatrix} \quad (8)$$

$$v_{Sn}^{CHE} = \frac{dx}{dt} = \frac{1}{C_{Sn,Cu} - C_{Sn,Cu_3Sn^+}} \times \begin{bmatrix} (n_{Sn,Cu}D_{Cu,Cu} + n_{Cu,Cu}D_{Sn,Cu})\frac{\partial C_{Sn,Cu}}{\partial x_{Cu}} \\ -(n_{Sn,Cu_3Sn}D_{Cu,Cu_3Sn} + n_{Cu,Cu_3Sn}D_{Sn,Cu_3Sn})\frac{\partial C_{Sn,Cu_3Sn}}{\partial x_{Cu_3Sn}} \end{bmatrix} \quad (9)$$

Equation 8 represents the flux velocity of a Cu atom moving from Cu to $Cu_3Sn$, due to chemical diffusion, and corresponds to arrow ① in Fig. 2. Using Eq. 8, the flux velocity of a Cu atom at the boundary of $Cu_3Sn/Cu_6Sn_5$ and $Cu_6S_5$/Sn can also be calculated, respectively, corresponding to arrows ② and ③ in Fig. 2. Using the same procedure, the flux velocity of a Sn atom that transfers due to chemical diffusion, is represented by Eq. 9.

## Variable Selection for Modeling

Effective charge number ($Z^*$) and diffusion coefficient ($D$) of Cu-Sn IMCs such as $Cu_3Sn$ and $Cu_6Sn_5$ are reported to have inconsistent values and limited resources.[19] However, consistent and reliable values of $Z^*$ and $D$, for Cu/Sn phases and Cu-Pb IMCs, have been reported in the literature.[19–23] Therefore, the variables to model Cu and Sn atoms in $Cu_3Sn$ and $Cu_6Sn_5$ were selected from the previous simulation study.[24–27] The variables used in the study are shown in Table II.

## Experimental Procedure to Observe Intermetallic Compound Growth by EM

The test specimen used in the EM experiment had the shape of a Cu-solder-Cu joint. Two Cu blocks of 3 mm × 10 mm × 15 mm were connected by applying Sn-0.7Cu solder paste to the middle of the blocks.[32] The solder layer had a thickness of approximately 170 $\mu$m after reflow soldering. The soldered specimen was wire-cut to a sandwich shape of 240 $\mu$m × 250 $\mu$m × 6170 $\mu$m, as shown in Fig. 3-a. The specimen was fixed by applying Pb-Sn solder to both ends of the test piece, as indicated in Fig. 3b.

**Table II. Coefficient values of Cu and Sn in a solder joint**

| Phase | Species | $D$ ($m^2$/s) | $Z^*$ | $Q^*$ (kJ/mol) | $R$ (Ω-nm) |
|---|---|---|---|---|---|
| Cu | Cu | $2.44 \times 10^{-29}$ [28] | 7 [20] | 21.34 [25] | 16.8 [31] |
| | Sn | $4.18 \times 10^{-27}$ [29] | 10 [24] | 1.36 [26] | |
| $Cu_3Sn$ | Cu | $9.2 \times 10^{-16}$ [24] | 30 [24] | 21.34 [25] | 89.3 [27] |
| | Sn | $5.3 \times 10^{-16}$ [24] | 32 [24] | 1.36 [26] | |
| $Cu_6Sn_5$ | Cu | $1.8 \times 10^{-15}$ [24] | 21 [24] | 21.34 [25] | 175 [35] |
| | Sn | $9.6 \times 10^{-16}$ [24] | 21 [24] | 1.36 [26] | |
| Sn | Cu | $2.01 \times 10^{-11}$ [30] | 2.5 [24] | 21.34 [25] | 115 [31] |
| | Sn | $4.59 \times 10^{-15}$ [28] | 18 [21] | 1.36 [26] | |

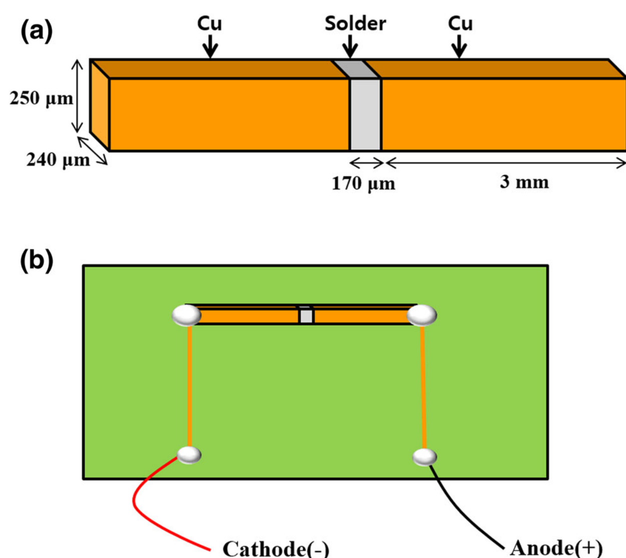


Fig. 3. Schematics of (a) test specimen and (b) current stressing method, for the EM experiments.[26]

Finally, a constant current of 6 A and a current density of 10 kA/cm$^2$ was applied to the test specimen. The EM test was conducted in a furnace at a temperature of 120°C. In order to investigate the IMC growth induced by EM, a temperature of 120°C was maintained, since the specimen increased to a temperature of approximately 120°C by applying a constant current of 6A. Moreover, the temperature of the solder bump in a practical package increases to 120–150°C due to joule heating.[33] Therefore, by using a test specimen of constant cross-sectional area (Fig. 3a), the effect of EM on IMC growth was investigated with a minimized TM contribution. IMC growth occurring in the Cu/solder interface was observed over the time period from when the EM test started (0 h, 25 h, 50 h, 100 h, 150 h, 200 h, 250 h and 300 h).

### Experimental Procedure to Observe Intermetallic Compound Growth by TM

Figure 4 shows the schematic diagram of the TM experimental setup. The hot plate (150°C) and the cooling module (55°C) were attached to the bottom

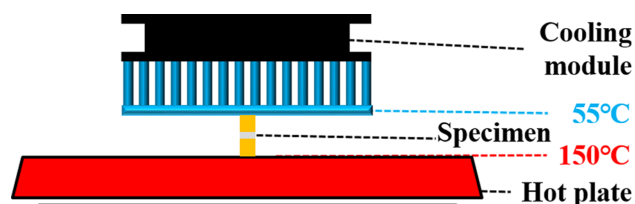


Fig. 4. Schematic diagram of the TM experiments.

and the top of the test specimen, respectively. The temperature of the cooling module was controlled by a temperature sensor, and a temperature variation of 55–150°C was maintained between the upper and lower sides. The TM experiment was conducted for 300 h.

The variation of IMC growth caused by EM and TM was observed from the cold-mounted specimen polished to 0.05 $\mu$m. This was followed by plating with Au film, and analyzing using back-scattered scanning electron microscopy (BS-SEM). The type of IMC was confirmed using energy dispersive spectroscopy (EDS). IMC growth normally has a non-uniform shape, containing corrugations and scallops. Therefore, the IMC thickness was calculated from the average area of IMC, divided by the linear width of the SEM images, taken from five images at the center of each specimen. The values of the IMC area, and linear width were acquired by image analysis.

## RESULTS AND DISCUSSION

### Intermetallic Compound Growth Under EM

Figure 5 shows the BS-SEM pictures of the IMCs grown at the interface between the Cu and solder under EM. Microstructures in Fig. 5 could be separated with a variation of black-white tone: white from Sn-rich solder, light gray from $Cu_6Sn_5$, medium gray from $Cu_3Sn$, and dark gray from the Cu pad. For quantitative evaluation of the $Cu_3Sn$ and $Cu_6Sn_5$ layers, EDS was conducted on the cross-section of the specimen, as shown in Fig. 6. P1 of dark gray was the Cu layer, P2 of medium gray was

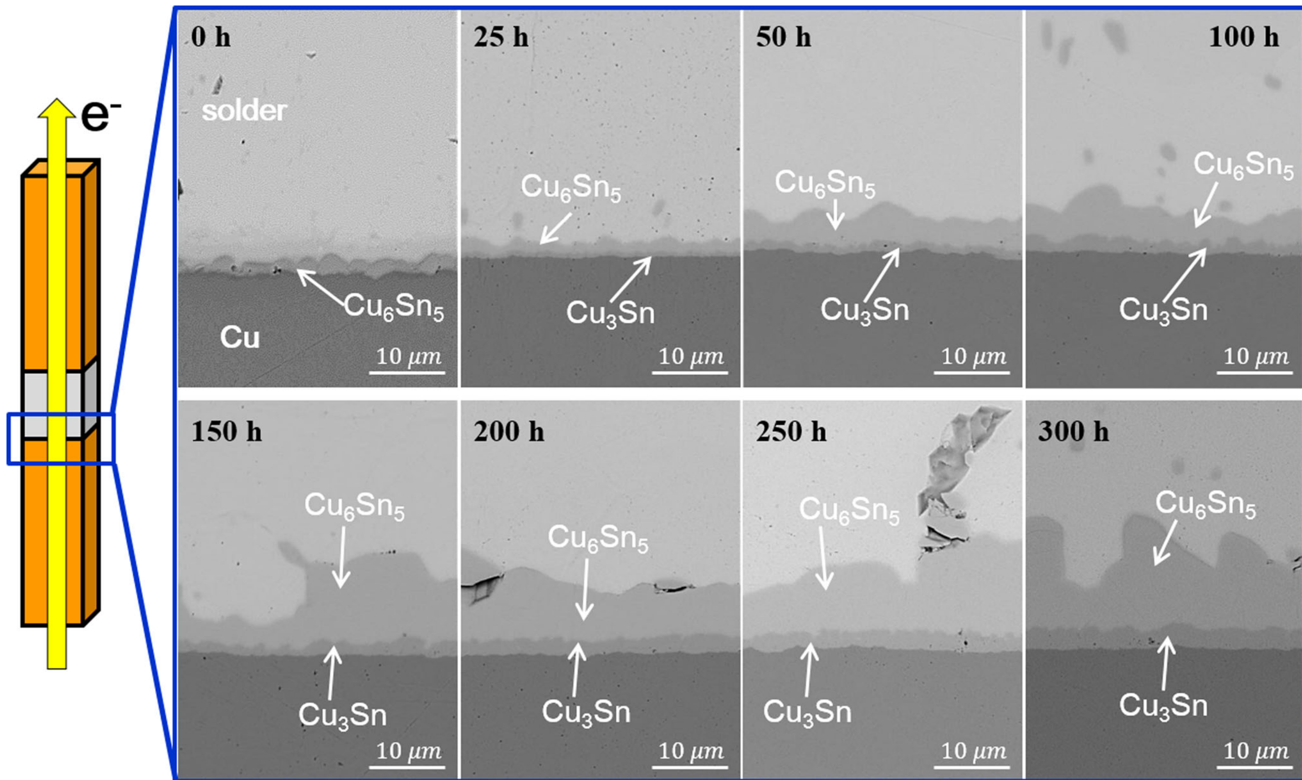


Fig. 5. BS-SEM image of an IMC grown by EM.

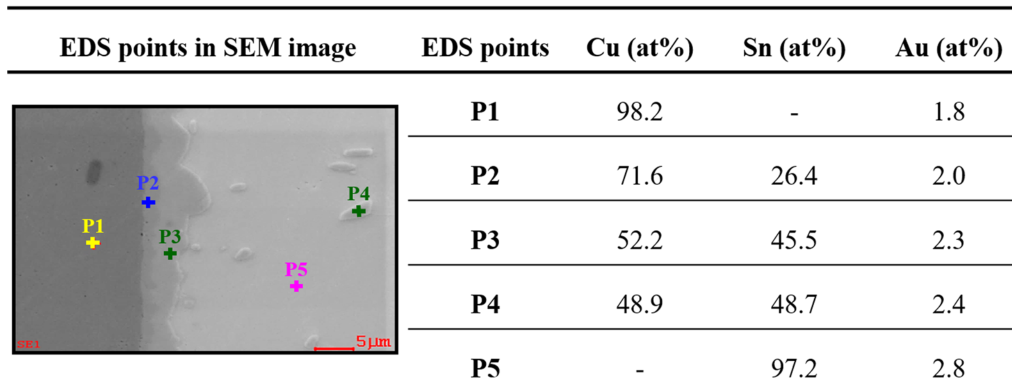

| EDS points in SEM image | EDS points | Cu (at%) | Sn (at%) | Au (at%) |
|---|---|---|---|---|
| | P1 | 98.2 | - | 1.8 |
| | P2 | 71.6 | 26.4 | 2.0 |
| | P3 | 52.2 | 45.5 | 2.3 |
| | P4 | 48.9 | 48.7 | 2.4 |
| | P5 | - | 97.2 | 2.8 |

Fig. 6. Chemical analysis of various microstructures in solder joints.

the $Cu_3Sn$ layer, P3 of light gray was the $Cu_6Sn_5$ layer, and P5 of white was the Sn-0.7Cu solder. An island phase of P4 was $Cu_6Sn_5$, which had grown apart from the P3 layer. The composition of Au was disregarded for phase analysis, because a thin layer of Au was intentionally coated on the sample to increase the resolution of the BS-SEM images. Before the EM test (0 h in Fig. 5), the IMC consisted mainly of $Cu_6Sn_5$. As the EM test continued to 25 h, an IMC of $Cu_3Sn$ appeared, and it had a thickness of 0.7 $\mu$m. Simultaneously, an IMC of $Cu_6Sn_5$ grew to 1.6 $\mu$m. During the 300 h of the EM test, $Cu_3Sn$ grew to 2.8 $\mu$m, and $Cu_6Sn_5$ to 11.3 $\mu$m. The IMCs continuously grew for the 300 h of the EM test, and the increase of the $Cu_6Sn_5$ thickness was more significant than that of the $Cu_3Sn$ thickness. The growth of IMCs by EM shows a similar trend to the previous study.[6] In particular, after 200 h in the EM test, a void was perceived at the interface between the $Cu_6Sn_5$ and the solder. This demonstrated the significance of the relationship between IMC growth and open circuit failure induced by void growth.[34]

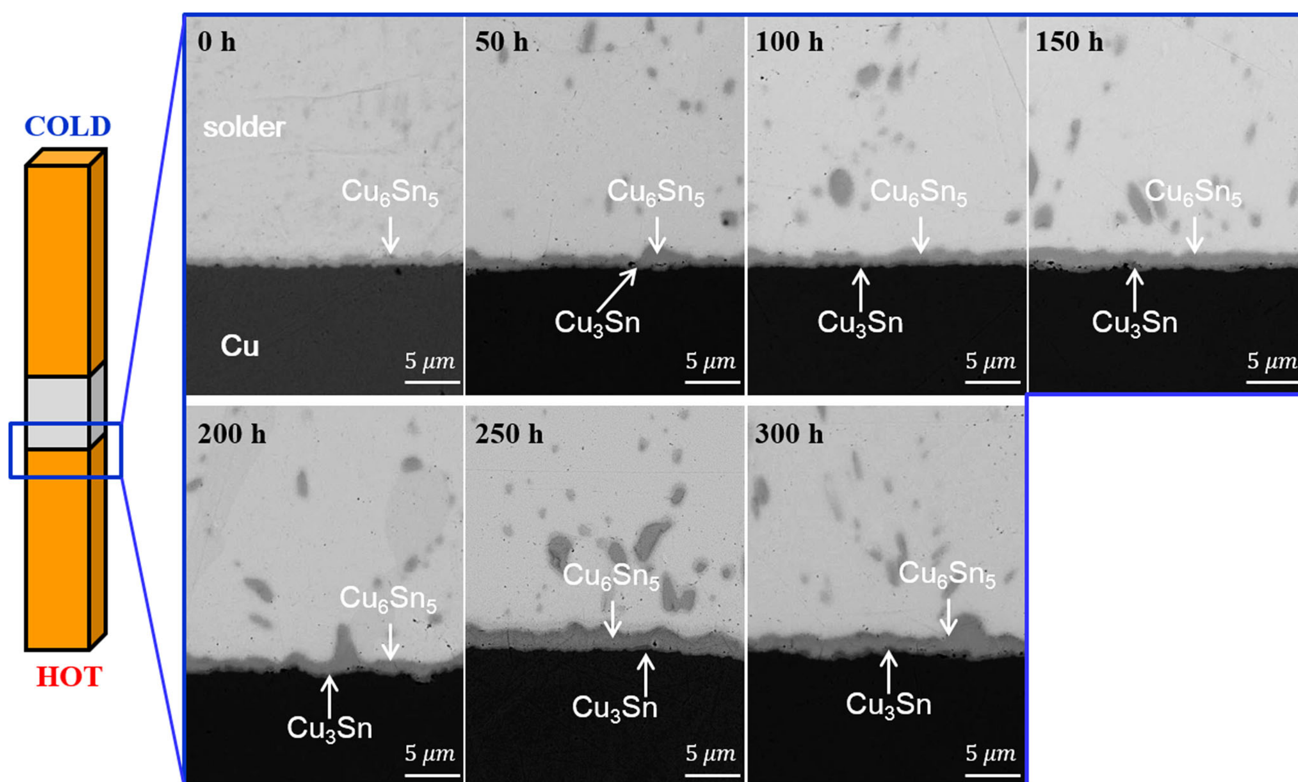


Fig. 7. BS-SEM image of an IMC grown by TM.

## Intermetallic Compound Growth Under TM

Figure 7 depicts the BS-SEM images of IMC growth between Cu and solder under TM. In the SEM image, unlike EM, the number of $Cu_6Sn_5$ islands increased during TM. At 50 h in the TM test, $Cu_6Sn_5$ that existed before the TM test had grown to a thickness of 1.1 $\mu$m. At this time, $Cu_3Sn$ first appeared in the TM test, and grew to 0.3 $\mu$m. At 300 h, $Cu_6Sn_5$ increased to 1.64 $\mu$m, and $Cu_3Sn$ to 0.53 $\mu$m. The IMC thickness increased proportionately with the time of TM test. However, the increase in thickness induced by TM, was significantly slower than that caused by EM. IMC growth induced by TM was conducted in the previous study. The results of previous TM studies were under the influence of EM and TM.[35,36] However, this study predicted IMC growth by TM without EM.

## Simulation to Measure the Thermogradient of a Solder Joint for TM

Thermogradient, one of important variables in the TM test, represented by $\left(-\frac{dT}{dx}\right)$ in Eq. 3, was calculated through finite element analysis, because the solder joint was too small to measure the temperature directly. Thermal analysis using ANSYS software was employed to estimate the temperature distribution.[36] The specimen for thermal simulation had the same size as the specimen used for the previous experiment (Fig. 3a). A temperature of 150°C was maintained at the lower heating side, and a temperature of 55°C was maintained at the upper cooling side. The convection coefficient and ambient temperature were 10 W/m$^2$ °C and 25°C, respectively. The variables to model Cu and the Sn-0.7Cu solder were selected from the previous simulation study.[27,31,37] The variables used in the study are shown in Table III.

Table III. Coefficient values of Cu and Sn-0.7Cu

| Phase | Thermal conductivity (W/m K) | *R* (Ω-nm) |
|---|---|---|
| Cu | 383[37] | 16.8[31] |
| Sn-0.7Cu | 53[37] | 89.3[27] |

Figure 8 shows the temperature distribution of a solder joint simulated by ANSYS.[36] The solder layer between the Cu rods indicated 102°C on the bottom and 95°C on the top. This translated to a temperature gap of 7°C over a distance of 170 $\mu$m, which produced a thermogradient of 870°C/cm in the solder layer. The thermogradient produced in this study is large enough to induce TM, because a thermogradient larger than 400°C/cm is required to cause TM phenomena.[38]

## Comparison of the Modeling and Experimental Results

Figure 9 shows both the predicted thickness of IMC growth through modeling and the measured thickness through the experiments. Specifically, Fig. 9a represents the IMC growth by EM under a current density of 10 kA/cm$^2$. The experimentally measured IMC thicknesses are noted with a filled rectangle for $Cu_6Sn_5$, and an open diamond for $Cu_3Sn$. Measuring the IMC thickness by BS-SEM (Fig. 5), $Cu_6Sn_5$ was thicker than $Cu_3Sn$. Moreover, $Cu_6Sn_5$ grew more rapidly than $Cu_3Sn$ under EM. The IMC thicknesses modeled for EM and TM are indicated with a solid line for $Cu_6Sn_5$ and a dotted line for $Cu_3Sn$. The EM-induced IMC thickness of $Cu_6Sn_5$ and $Cu_3Sn$ successfully matched the experimental values. Previous studies on EM and IMC growth[4,5,12] dealt with a solder bump packaged on flip-chip ball grid arrays (FC-BGA). Therefore, the cross-sectional area of a bump entrance was narrower than that of the Cu-pad, producing current crowding at the entrance to the solder bump.[39] The complicated phenomena of EM and TM caused the estimations for a practical solder bump of an FC-BGA to differ from the observed IMC thickness. However, the test specimen used in this study had a constant thickness, and the atom transfer was always in the vertical direction, to the boundaries of the Cu-solder-Cu specimen. Thus, by using our specimen geometry, the effect of current crowding on both the joule heating and IMC growth were minimized (Fig. 3a). Moreover, the EM test conducted at the constant temperature of 120°C, minimized the thermogradient, and ultimately the TM effects on IMC growth through the EM specimen. This is why our study produced a very good agreement between the modeled IMC growth and the experimental IMC thickness.

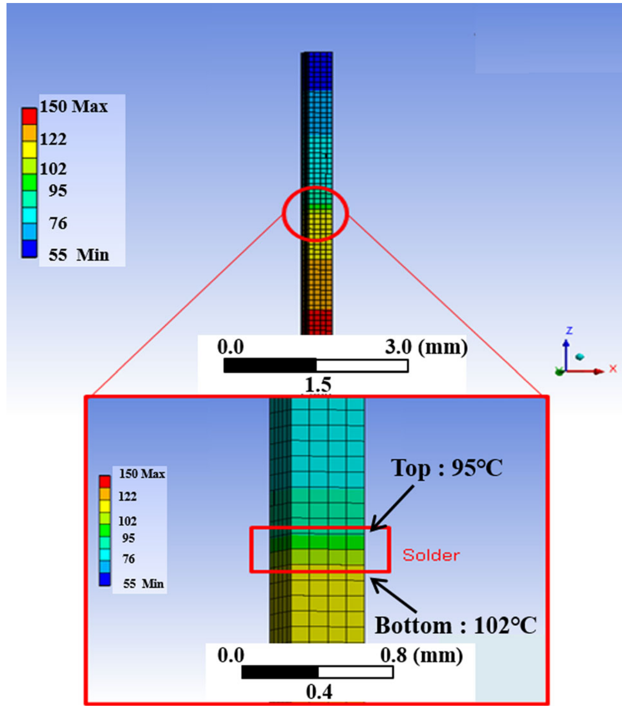


Fig. 8. Temperature distribution in a solder joint (The inset is the enlarged view of the solder layer between the Cu rods.).

Figure 9b shows the IMC growth induced by TM under a thermogradient of 870°C/cm. The TM simulation and experiments both indicated the same behavior of the IMC growth increasing with time. Furthermore, following the experimental IMC behavior (Figs. 5 and 7), the growth velocity of IMC ($Cu_6Sn_5$ and $Cu_3Sn$) affected by TM was much slower than that induced by EM. The simulated IMC thickness showed a good agreement with the measured values, and the thickness of $Cu_6Sn_5$ was simulated to increase more rapidly than that of

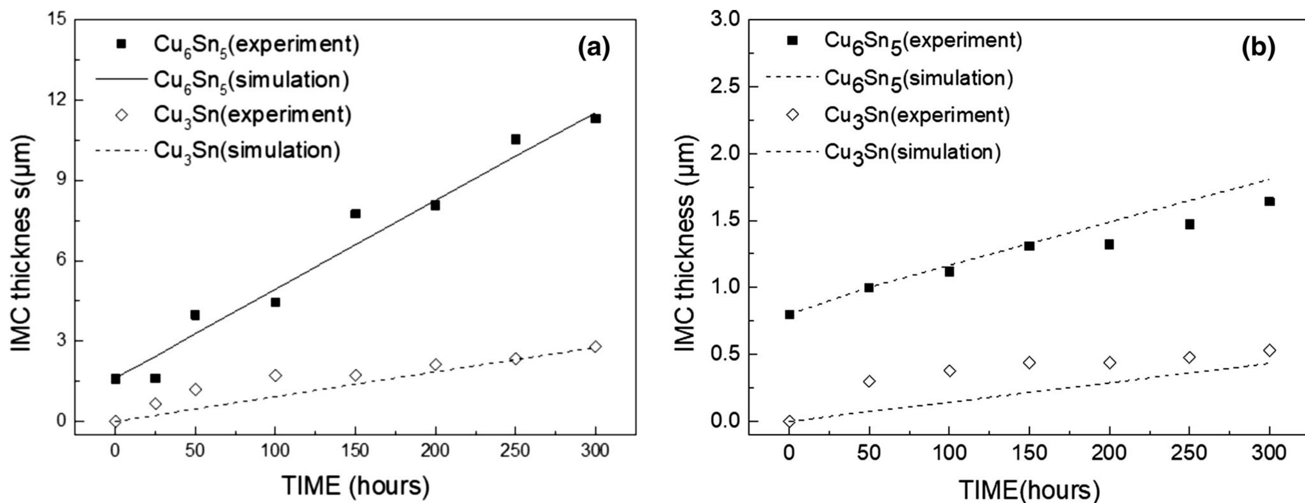


Fig. 9. Comparison of modeling and experimental thickness of IMCs grown under (a) EM and (b) TM.

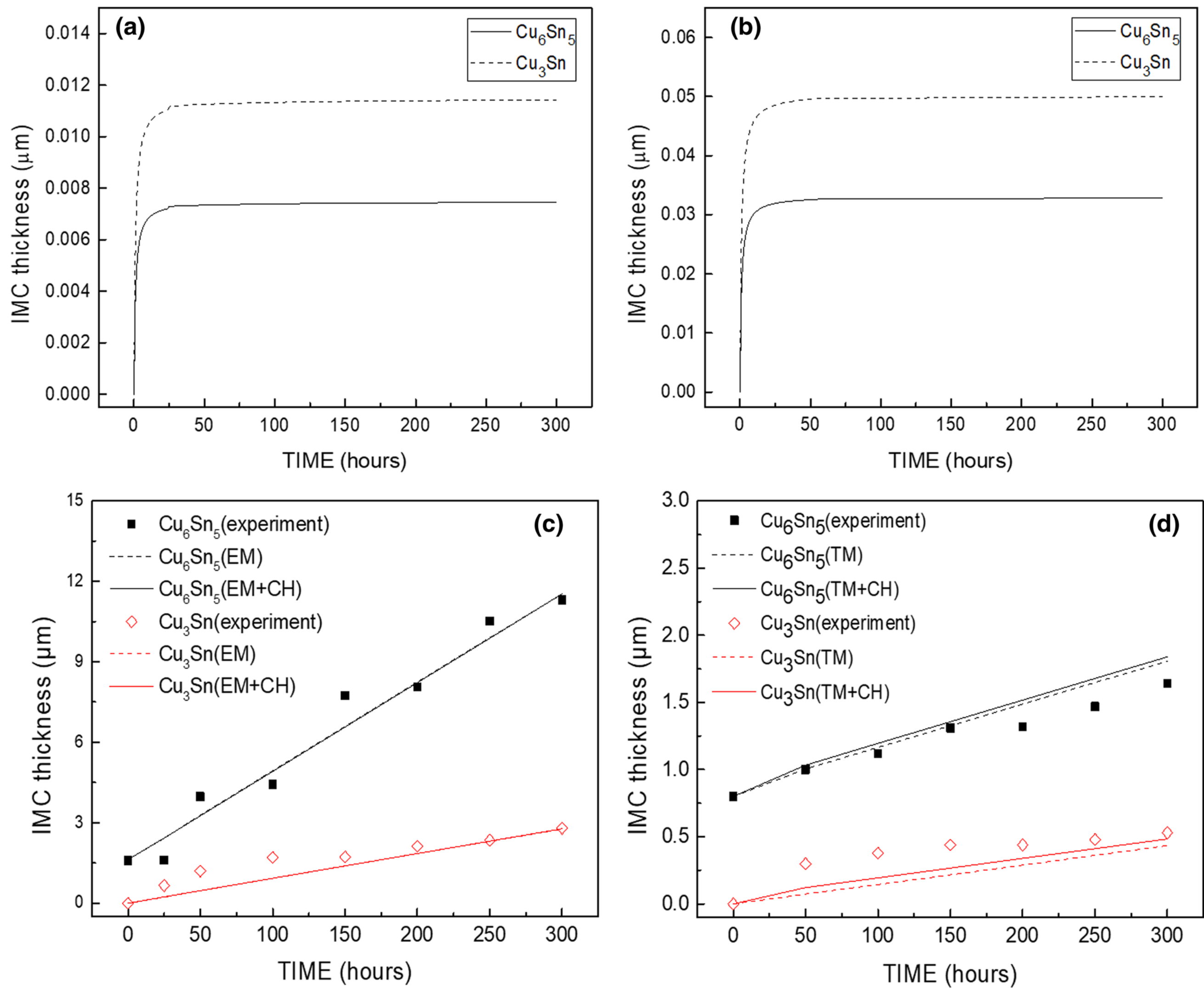


Fig. 10. Effect of chemical diffusion on IMC growth: (a) chemical diffusion under EM, (b) chemical diffusion under TM, (c) EM combined with chemical diffusion, and (d) TM combined with chemical diffusion.

$Cu_3Sn$. Specifically, the estimation of $Cu_6Sn_5$ was coincident with the measured value at 150 h. However, the measured thickness of $Cu_6Sn_5$ was 14% lower than the predicted values (by modeling), from 200 h onwards. This difference between the modeled and experimental values can be explained by the significant formation of a $Cu_6Sn_5$ island, which was separated from the IMC continuous layers, and therefore, not included in the measured thickness of the IMC. Also, the reason for the underestimation of $Cu_3Sn$, is that $Cu_6Sn_5$ is first formed in the Cu-solder interface, and $Cu_3Sn$ is formed afterwards. In our modeling, it was assumed that $Cu_3Sn$ and $Cu_6Sn_5$ form at the same time.

The contribution of chemical diffusion on IMC growth was comparatively calculated from the measured IMC thickness induced by EM and TM, respectively. The IMC thicknesses (measured every 50 h) were substituted into Eq. 8, and an interim growth of IMC, within the 50 h time periods was considered to follow a linear relationship. For Eq. 8, if $x_{Cu_3Sn}$ (the thickness of $Cu_3Sn$ induced by EM and TM) increases, $J_{Cu_3Sn}$ decreases. Therefore, the atomic flux of Cu decreases as $Cu_3Sn$ thickens. If $x_{Cu_6Sn_5}$ (the thickness of $Cu_6Sn_5$ affected by EM and TM) increases, $J_{Cu_6Sn_5}$ decreases. Therefore, the atomic flux of Cu decreases as $Cu_6Sn_5$ thickens.

Figure 10a shows the contribution of chemical diffusion on IMC growth induced by EM. The contribution of chemical diffusion on the thickness of $Cu_3Sn$ ($x_{Cu_3Sn}$) was more significant than that of $Cu_6Sn_5$ ($x_{Cu_6Sn_5}$). In Fig. 8a, the growth of $Cu_6Sn_5$ (induced by EM) was larger than that of $Cu_3Sn$. Therefore, $J_{Cu_6Sn_5}$ (the atomic flux of Cu in the $Cu_6Sn_5$ phase) was relatively less affected by chemical diffusion than $J_{Cu_3Sn}$. However, the contribution of chemical diffusion (on IMC growth induced by EM) was 0.007–0.011 $\mu$m, and it was insignificant

compared to the thickness of $Cu_6Sn_5$ and $Cu_3Sn$ growth.

Figure 10b indicates the contribution of chemical diffusion on IMC growth induced by TM. For the same reason discussed in Fig. 10a, the contribution of chemical diffusion on the thickness of $Cu_3Sn$ ($x_{Cu_3Sn}$) was more significant than that of $Cu_6Sn_5$ ($x_{Cu_6Sn_5}$). The contribution of chemical diffusion on IMC growth (induced by TM) was 0.03–0.05 $\mu$m, and it was approximately six times larger than the chemical diffusion contribution on IMC growth induced by EM. That was because the IMC thickness induced by TM was smaller than that by EM (Fig. 9).

Figure 10c and d represent the total thickness of IMCs, induced by EM and TM combined with chemical diffusion, respectively. The IMC thickness measured experimentally is denoted with a filled rectangle for $Cu_6Sn_5$, and an open diamond for $Cu_3Sn$. The IMC thicknesses induced by EM and TM are indicated with black and red dotted lines for $Cu_6Sn_5$ and $Cu_3Sn$, respectively. EM and TM combined with chemical diffusion are denoted by black and red solid lines for $Cu_6Sn_5$ and $Cu_3Sn$, respectively. The IMC growth caused by EM and chemical diffusion combined, was mostly the same as that by EM alone, because the contribution of chemical diffusion to IMC growth under EM was insignificant, as shown in Fig. 10a. However, the contribution of chemical diffusion on the IMC growth induced by TM was significant, as shown in Fig. 10-d. Incorporating chemical diffusion with TM, $Cu_3Sn$ growth increased by 10%, and $Cu_6Sn_5$ by 4%. Specifically, the difference between the predicted and measured $Cu_3Sn$ thickness was improved by considering chemical diffusion under TM. Therefore, the effect of chemical diffusion was significant on IMC growth induced by TM.

## CONCLUSION

This study predicted IMC growth behavior modeled from electromigration (EM), thermomigration (TM), and chemical diffusion, for Sn-0.7Cu solders. IMC thickness, modeled under a current density of 10 kA/cm$^2$, showed a good agreement with the measured value. This might be because a test specimen with constant thickness was used in the EM test, to remove the effects of both current crowding and TM on the EM specimen. TM modeling produced the same trend of IMC growth when compared with the experimental measurements. However, $Cu_6Sn_5$ thickness modeled by TM made an overestimation of 14% in comparison to the measured values. This discrepancy can be explained by the significant formation of a $Cu_6Sn_5$ island, which was separated from the IMC continuous layers and not included in the measured thickness of IMC. The reason for the $Cu_3Sn$ underestimation is that $Cu_3Sn$ and $Cu_6Sn_5$ are assumed to be formed at the same time. We have determined that the IMCs of $Cu_3Sn$ and $Cu_6Sn_5$ grew more significantly by EM than by TM/chemical diffusion. Modeling of TM should reflect the chemical diffusion effect on the IMC growth. TM incorporated with chemical diffusion increased IMC growth of $Cu_3Sn$ by 10%, and $Cu_6Sn_5$ by 4%. Moreover, chemical diffusion had little influence on IMC growth by EM. The test specimen used for the study of EM and TM was very beneficial for understanding IMC growth behavior. The specimen had a constant thickness, and transferred the electrons/atoms in a vertical direction to the boundaries of the Cu-solder-Cu specimen. Thus, the effect of current crowding on both the joule heating and IMC growth were minimized to better understand the effect of EM and TM on IMC growth.

## ACKNOWLEDGMENTS

This work was supported by the National Research Foundation of Korea (NRF) Grant Funded by the Korea government (MSIT) through GCRC-SOP (Grant No. 2011-0030013).

## REFERENCES


1. E.C.C. Yeh, W.J. Choi, and K.N. Tu, *Appl. Phys. Lett.* 80, 580 (2002).
2. S.W. Liang, Y.W. Chang, and C. Chen, *Appl. Phys. Lett.* 88, 172108 (2006).
3. S.H. Chiu, T.L. Shao, and C. Chen, *Appl. Phys. Lett.* 88, 022110 (2006).
4. R. Labie, P. Limaye, K.W. Lee, C.J. Berry, E. Beyne, and I.D. Wolf, in *3rd Electronics System Integration Technology Conference ESTC*, pp. 1–5 (2010).
5. F. Ouyang, H. Hsu, Y. Su, and T. Chang, *J. Appl. Phys.* 112, 023505 (2012).
6. B.H. Chao, X. Zhang, S. Chae, and P.S. Ho, *Microelectron. Reliab.* 49, 253 (2009).
7. S. Chae, X. Zhang, K. Lu, H. Chao, P.S. Ho, M. Ding, P. Su, T. Uehling, and L.N. Ramanthan, *J. Mater. Sci. - Mater. Electron.* 18, 247 (2007).
8. H. Gan and K.N. Tu, *J. Appl. Phys.* 97, 063514 (2005).
9. S. Chae, B. Chao, X. Zhang, J. Im, and P.S. Ho, in *57th Electronic Components and Technology Conference*, pp. 1442–1449 (2007).
10. W.K. Choi and H.M. Lee, *J. Electron. Mater.* 29, 1207 (2000).
11. J. Yoon and S. Jung, *J. Mater. Sci.* 39, 4211 (2004).
12. C.Y. Liu, L. Ke, Y.C. Chuang, and S.J. Wang, *J. Appl. Phys.* 100, 083702 (2006).
13. L. Xu, J.H.L. Pang, K.H. Prakash, and T.H. Low, *IEEE Trans. Compon. Packag. Technol.* 28, 408 (2005).
14. K. Yamanaka, Y. Tsukada, and K. Suganuma, *Microelectron. Reliab.* 47, 1280 (2007).
15. C. Chen, H.M. Tong, and K.N. Tu, *Annu. Rev. Mater. Res.* 40, 531 (2010).
16. L.S. Darken, *Metall. Mater. Trans. B* 41, 277 (2010).
17. P. Shewmon, *Thermo- and electrotransport in solids* (Warrendale: TMS, 1989) chapter 7.
18. N. Saunders and A.P. Miodownik, *Binary Alloy Phase Diagram*, ed. T.B. Massalski (Russell Township: ASM International, 1990), p. 1481.
19. B. Chao, S. Chae, X. Zhang, K. Lu, J. Im, and P.S. Ho, *Acta Mater.* 55, 2805 (2007).
20. G.A. Sullivan, *J. Phys. Chem. Solids* 28, 347 (1967).
21. A. Khosla and H.B. Huntington, *J. Phys. Chem. Solids* 36, 395 (1975).
22. R. Grone, *J. Phys. Chem. Solids* 20, 88 (1961).
23. M.Y. Hsieh and H.B. Huntington, *J. Phys. Chem. Solids* 39, 867 (1978).

24. H.L. Chao, Ph.D. Thesis, The University of Texas at Austin, Texas (2009).
25. W. Hsu and F. Ouyang, *Mater. Chem. Phys.* 165, 66 (2015).
26. H. Hsiao and C. Chen, *Appl. Phys. Lett.* 94, 092107 (2009).
27. C. Wei, C.F. Chen, P.C. Liu, and C. Chen, *J. Appl. Phys.* 105, 023715 (2009).
28. W. Seith and T. Heumann, *Diffusion of Metals: Exchange Reactions* (Berlin: Springer, 1962), p. 65.
29. K. Hoshino, Y. Iijima, K. Hirano, and T. Jpn, *I. Met.* 21, 674 (1980).
30. F. Dyson, T.R. Anthony, and D. Turnbull, *J. Appl. Phys.* 38, 3408 (1967).
31. P. Yang, C. Kuo, and C. Chen, *JOM* 60, 77 (2008).
32. K. Lee, K. Kim, and K. Suganuma, *J. Mater. Res.* 26, 2624 (2011).
33. Y. Kim, S. Nagao, T. Sugahara, K. Suganuma, M. Ueshima, and H. Albrecht, *J. Mater. Sci. - Mater. Electron.* 25, 3090 (2014).
34. B. Chao, S. Chae, X. Zhang, K. Lu, M. Ding, J. Im, and P.S. Ho, *J. Appl. Phys.* 100, 084909 (2006).
35. H. Ye, C. Basaran, and D. Hopkins, *Appl. Phys. Lett.* 82, 1045 (2003).
36. S.H. Chiu, S.W. Liang, C. Chen, D.J. Yao, Y.C. Liu, K.H. Chen, and S.H. Lin, in *56th Electronic Components and Technology Conference*, p. 4 (2006).
37. T. Chellaih, G. Kumar, and K.N. Prabhu, *Mater. Des.* 28, 1006 (2007).
38. A.T. Huang, A.M. Gusak, and K.N. Tu, *Appl. Phys. Lett.* 88, 141911 (2006).
39. L. Zhang, S. Ou, J. Huang, and K.N. Tu, *Appl. Phys. Lett.* 88, 012106 (2006).